Int J Adv Manuf Technol (2017) 90:699–708
DOI 10.1007/s00170-016-9397-3

ORIGINAL ARTICLE

Prediction of surface roughness ratio of polishing blade of abrasive cloth wheel and optimization of processing parameters

Wenbo Huai[1] · **Hong Tang**[1] · **Yaoyao Shi**[1] · **Xiaojun Lin**[1]

Received: 2 May 2016 / Accepted: 29 August 2016 / Published online: 7 September 2016
© Springer-Verlag London 2016

Abstract Abrasive cloth wheel is significantly flexible at high-speed rotation and could realize adaptive micro-surface contact polishing of the blade of aviation engines. To reduce surface roughness and improve the surface integrity and mechanical property of the blade of aviation engine, this study determined the primary and secondary processing parameters by using orthogonal test and range method. Results show a significant linear correlation between blade surface roughness before and after polishing. A range of polishing parameters for orthogonal central combination test was determined based on the tendency chart. A roughness ratio prediction model was established based on the orthogonal central combination test results. This model was verified significant by variance and diversity analyses. The polishing parameters were optimized using response surface method. Finally, polishing experiment using a blisk confirmed the reliability of the established prediction model and the optimized parameters.

Keywords Abrasive cloth wheel · Blade of aviation engine · Flexible polishing · Roughness ratio · Prediction model

1 Introduction

Surface roughness influences the functional characteristics, fatigue durability, and surface friction properties of a workpiece [1]. The blade of an aviation engine presents an unqualified surface roughness and easily suffers from fatigue failure, deformation, or breakage under high-temperature and high-pressure service environments [2], resulting in incredible consequences. Machine-shaping blade is a spatial freeform surface with evident milling remain height [3]. Therefore, polishing technology is needed to remove remains and achieve satisfactory surface roughness [4], improving blade surface quality and performance of aircraft engine. Studies have focused on spatial complex surface polishing and achieved outstanding results.

Robots [5, 6] and computer numerical control (CNC) machines [7] are widely used as polishing machines in foreign countries. These machines demonstrate ideal effect on complex surfaces when combined with route planning [7] and visual positioning [5] technologies. However, CNC machines are expensive and their polishing force cannot be controlled [8]; by contrast, robots display considerable polishing track errors [5]. Pan et al. [8], Zeng and Blunt [9], and Ji [10] of Zhejiang University of Technology used gas bag as polishing tool for spherical lens, medical cobalt-chromium alloy, and mold surface. Results showed that ideal polishing effect can be obtained by controlling the processing parameters. Academic circles have proposed some non-contact polishing techniques for complex geometries, such as magnetofluid [11], abrasive fluid [12], and electrofluid [13, 14]. However, these techniques demonstrate small material removal rate, low polishing efficiency [11], and high cost [15]. An abrasive belt [16, 17] is used as the main polishing tool because of its high polishing efficiency, although this tool is inapplicable in blisk in narrow vent passage because of its large grinding head [18, 19].

Abrasive cloth wheel can be used to polish blisks in narrow vent passages because of its small volume, simple structure, and flexibility. In previous study, a blade was polished using an abrasive cloth wheel in an independently developed five-

✉ Wenbo Huai
qjjxk@sohu.com

[1] The Key Laboratory of Contemporary Design and Integrated Manufacturing Technology, Ministry of Education, Northwestern Polytechnical University, Xi'an 710072, China

axis CNC machine to reduce interference and improve the adaptivity and polishing efficiency of "shape-followed contact" between the grinding tool and the polishing surface [20]. The radius of the abrasive cloth wheel at high-speed rotation increases under centrifugal force, demonstrating the good elasticity of this tool; hence, abrasive cloth wheel can realize the "shape-followed contact" on the surface during polishing. This technique can avoid "under-polishing" or "over-polishing" while maintaining stable polishing force, thereby increasing the polishing efficiency. Nevertheless, the influence of the processing parameters of abrasive cloth wheel on surface roughness, coupling mechanism, prediction model, and optimization of processing parameters remains unknown.

Numerous studies have investigated surface roughness prediction. Yong [21] established a surface roughness model of nano-crystalline hydroxyapatite milling by using polycry stalline diamond insert in milling test and the optimized processing parameters by using Minitab software. Ho et al. [1] constructed a milling surface roughness prediction model by using adaptive fuzzy genetic algorithm. Hanafi et al. [22] studied the coupling effect of cutting speed, cutting depth, and feed speed on surface roughness of poly ether ether ketone CF30 milling by using the artificial neural network approach and then established a surface roughness prediction model. Zhao [16] applied the response surface method and established a surface roughness prediction model for abrasive band polishing of blade of aviation engine. Using aluminum alloy milling with a monocrystal diamond cutter, Singh [23] established a surface roughness prediction model through regression analysis. Bigerelle [24] effectively predicted the surface roughness of clutch gear in abrasive band grinding though fractal function simulation, which reduced the number of tests. By using magnetic-assisted aluminum polishing, Givi et al. [14] established a roughness prediction model by using the orthogonal test method. Among these methods, the response surface method is superior to neural network algorithm, genetic algorithm, and SNR design approach in terms of fitting precision and fitting efficiency [16]. Therefore, this study employed the surface response method to optimize the processing parameters of the abrasive cloth wheel.

Moreover, these methods only predict surface roughness and they do not clearly indicate the correlation of surface roughness before and after polishing. The surface roughness of milled blades of aviation engine differs significantly, and the author found from test results that when similar processing parameters are applied to blades with different roughness, different polishing effects will be achieved. To address this problem, this study established a surface roughness ratio prediction model and optimized the parameters by using the response surface method. First, primary and secondary processing parameters were determined via a range test involving the orthogonal test. Influence law of a single processing parameter on roughness ratio was analyzed based on a tendency chart, and the correlation analysis revealed a significant correlation between surface roughness before and after polishing. Second, a regression model between processing parameters and roughness ratio was constructed based on the orthogonal central combination test results, which verified the significance of the model. Third, based on the prediction model, the processing parameters were optimized by using the response surface method. Last, the established model and optimized parameters were verified through a polishing test using a blisk.

2 Polishing test

2.1 Test platform

For polishing, this study used an independently developed five-axis CNC machine (Fig. 1), which consists of three rectilinear coordinate axes and three rotational coordinate axes. These axes of motion include rectilinear axes (X, Y, and Z), rotational axis of blade (U), swing axis of blade (C), and swing axis of flexible grinding head (A). The principal axis A allows for real-time adjustment of the grinding head pose involving three micro-displacement cylinders in radial uniform distribution and one axial micro-displacement cylinder according to the changes in blade geometric profile in the CNC program, which protects effective contact between the abrasive cloth wheel and the blade geometric profile, thus realizing flexible adaptive polishing. The working principle is introduced in Reference [20].

This test used 10 TC4 blade samples (A–J) (Fig. 2). The back and basin of every blade were divided into three zones from the root to the tip, numbered 1, 2, and 3, respectively. For

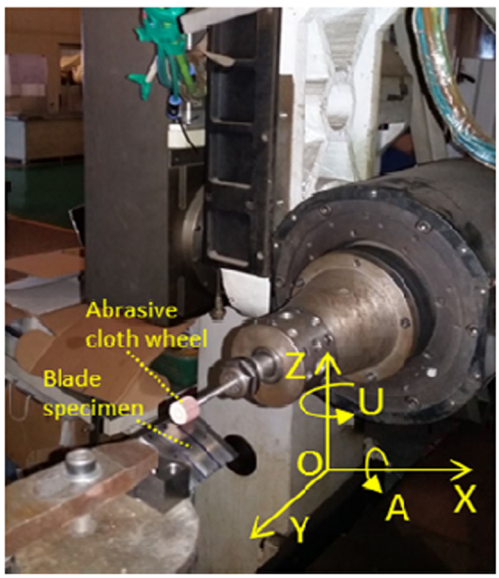

Fig. 1 Five-axis CNC polishing machine

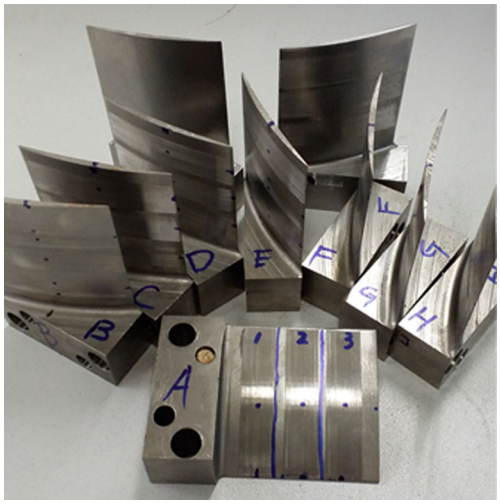

Fig. 2 TC4 blade samples

example, three zones on the back of blade A were marked A1, A2, and A3.

The characteristic of TC4 includes easy adhesion, high grinding temperature, strong chemical activity, and low grinding ratio during grinding. Considering the demands for adequate flexibility of the abrasive cloth wheel during polishing, this paper chose an 8.5 mm × 14 mm × P (initial radius r-$_0$ × thickness L × abrasive size P) (P = 60#, 240#, 320#, 400#, 600#) green SiC (GC) cloth-based abrasive cloth wheel as grinding tool. A new abrasive cloth wheel was used in each case wherein the experimental time is approximately 4–6 min, which lies within the effective life of an abrasive cloth wheel (25–30 min).

Five measuring points were randomly chosen from the polishing zones before and after polishing. Surface roughness was measured by a Mar Surf XR 20 surface roughometer (sampling length = 0.8 mm and evaluation length = 4 mm) by using the vertical polishing track approach. The mean value was considered the final result.

2.2 Analysis of processing parameters

Figure 3(a) shows that under the influence of centrifugal force, radius r (mm) of the abrasive cloth wheel increases from initial radius r_0 to $r_0 + \Delta r$ as it rotates at the speed of ω (r/min). The abrasive cloth wheel suffers from radial compression from the polishing surface. The rotation speed (ω) and amount of compression (a_p/mm) are the main influencing parameters of the polishing force [2] and the key processing parameters that influence surface roughness [3]. Figure 3(b) shows that line spacing between polishing routes (p/mm) determines polishing number n ($n = L/p$). Feed speed (v_f/mm/min) and abrasive size (P) influence the number of abrasive particles involved in polishing [3]. Therefore, the processing parameters of abrasive cloth wheel include ω, a_p, v_f, P, and p.

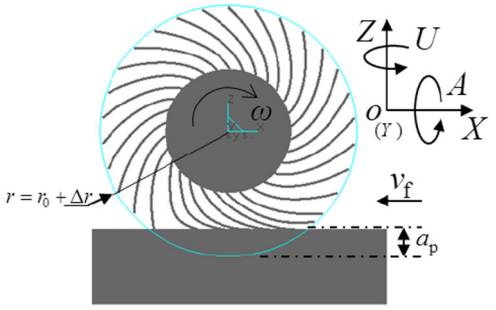

(a) Amount of compression (a_p / mm)

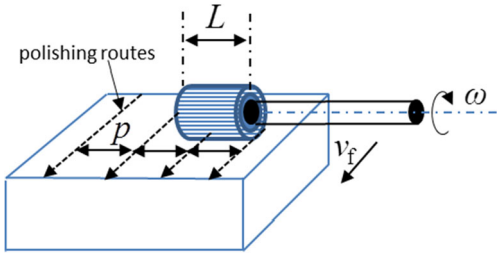

(b) Spacing between polishing routes (p /mm)

Fig. 3 Polishing principle. **a** Amount of compression (a_p/mm). **b** Spacing between polishing routes (p/mm)

Isoparametric line method [19] was employed in track planning, and the cutter radius in CNC programming was r-a_p, ensuring that the abrasive cloth wheel displays a stable amount of compression during polishing. Given that horizontal line spacing method can effectively eliminate external waviness of the blade [20], horizontal line spacing-based polishing, that is, polishing along the milling track, was employed in this study. Figure 4 shows the relationship between ω and r in abrasive cloth wheel with an initial radius of r_0.

To explore the influence law of processing parameters of the abrasive cloth wheel on surface roughness and their importance order, this study designed a five-factor three-level orthogonal test to assess the polishing effect on the backs of blades A–H. The test results are listed in Table 1. y is the roughness ratio after and before polishing: $y = R'_a/R_a$. K_i is the sum of row i in all columns: $k_i = K_i/s$, where s is frequency of occurrence of different factor levels on any column.

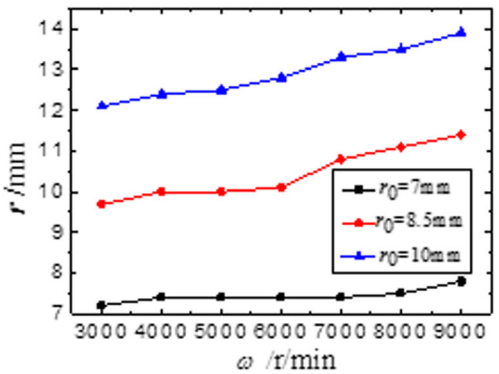

Fig. 4 Relationship between radius and rotation speed of the abrasive cloth wheel

Table 1 Experimental results using central composite design

Number	ω/r/min	p/mm	a_p/mm	v_f mm/min	P	Polishing area	R_a	R'_a	y
1#	4500	0.7	0.6	320	60	D3	1.1135	2.3166	2.080
2#	4500	1.2	0.9	220	600	C2	1.9043	1.4095	0.740
3#	4500	1.7	1.2	120	320	G1	1.8420	1.2372	0.672
4#	6000	0.7	0.6	220	600	B3	1.0941	1.2248	1.119
5#	6000	1.2	0.9	120	320	G2	1.8186	0.7658	0.421
6#	6000	1.7	1.2	320	60	A1	2.0806	1.6677	0.802
7#	7500	0.7	0.9	320	320	E3	1.3498	0.6370	0.472
8#	7500	1.2	1.2	220	60	D2	1.0809	3.3880	3.134
9#	7500	1.7	0.6	120	600	C1	1.9391	1.7283	0.891
10#	4500	0.7	1.2	120	600	C3	2.1003	1.2601	0.600
11#	4500	1.2	0.6	320	320	E2	1.5610	1.1202	0.718
12#	4500	1.7	0.9	220	60	D1	2.0061	3.2663	1.628
13#	6000	0.7	0.9	120	60	A3	1.4984	1.5567	1.039
14#	6000	1.2	1.2	320	600	B2	1.5572	1.1864	0.762
15	6000	1.7	0.6	220	320	E1	1.9691	1.3003	0.660
16#	7500	0.7	1.2	220	320	G3	1.8591	0.5510	0.296
17#	7500	1.2	0.6	120	60	A2	1.8242	1.1607	0.636
18#	7500	1.7	0.9	320	600	B1	2.0662	1.8200	0.881
19#	6000	1.2	0.9	220	320	H1	2.1398	1.3758	0.643
20#	6000	1.2	0.9	220	320	H2	1.8867	1.2213	0.647
21#	6000	1.2	0.9	220	320	H3	1.2445	0.7931	0.637
22#	6000	1.2	0.9	220	320	F1	2.0566	1.1422	0.555
23#	6000	1.2	0.9	220	320	F2	1.9704	1.2551	0.637
24#	6000	1.2	0.9	220	320	F3	2.0863	1.3935	0.668
K_1	1.07	0.97	1.02	0.95	1.55				
K_2	0.73	0.86	0.76	0.96	0.61				
K_3	1.09	0.92	1.08	0.73	0.83				
R	0.35	0.11	0.32	0.23	0.72				

Therefore, k_i is the arithmetic mean of all test results under level i. In this paper, $s = 3$. R is the range, $R = \max(K_1, K_2, K_3) - \min(K_1, K_2, K_3)$ or $R = \max(k_1, k_2, k_3) - \min(k_1, k_2, k_3)$. A large range implies that changes in numerical value in the current column of factors will greatly affect the test results. Hence, the column showing the biggest range is the primary factor. As shown in Table 1, P is the primary influencing factor of roughness ratio, followed by ω, a_p, v_f, and p successively. Figure 5 shows the tendency chart which uses the factor levels as horizontal coordinate and the range as vertical coordinate. The tendency chart reflects variation trend in roughness ratio as factor values (processing parameters) increases.

2.3 Design of the orthogonal central combination test

The central combination test ranges of ω, a_p, v_f, and p could be determined according to Fig. 5, as follows: 5000–7000 r/min, 0.6–1.2 mm, 120–200 mm/min and 240#–400#, respectively. Based on the above analysis, p is the least important influencing factor of surface roughness. To reduce the number of tests, p could be fixed at a good level, i.e., $p = 1.2$ mm. Table 2 shows the factor levels of the orthogonal central combination test, and Table 3 shows test programs and results. The orthogonal central combination test aimed to polish the basins of blades A–J.

3 Analysis of test results

3.1 Roughness ratio prediction model

Due to vibration of machining tools and system error, profiles of blades milled under same processing parameters will display significantly different errors and surface roughness. Similarly, blades polished under same processing parameters will show different surface roughness. According to six groups of zero-level test results

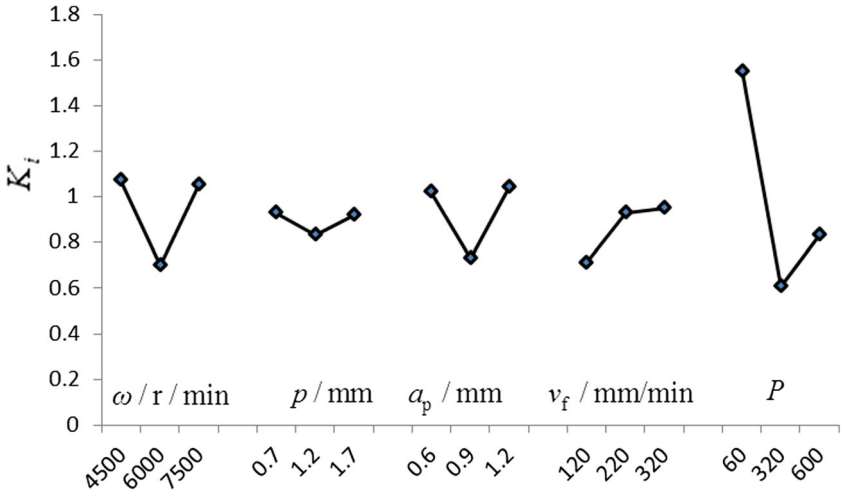

Fig. 5 Trend chart

(Table 1), six blades with different surface roughness display different surface roughness after polishing. The correlation coefficient between surface roughness before (R_a) and after (R'_a) the polishing is $\rho = 0.932$, indicating a significant positive linear correlation. Therefore, roughness ratio can better reflect the effects of processing parameters on polishing performance, especially in rough polishing. Roughness ratio is more suitable for parameter optimization compared with surface roughness. The roughness ratio predicted by the established prediction model was $y = R'_a/R_a$.

Surface roughness is the coupling effect of processing parameters and the prediction model of surface roughness is nonlinear. Therefore, the established prediction model can be expressed as:

$$y = y - \varepsilon = a + \sum_{j=1}^{m} b_j x_j + \sum_{k<j} b_{kj} x_k x_j + \sum_{j=1}^{m} b_{jj} x_j^2, k = 1, 2, ..., m-1 (j \neq k) \quad (1)$$

where y is the predicted value of roughness ratio, y is the roughness ratio, ε is the prediction error, a and b are the regression coefficients of the prediction model, x is a processing

Table 2 Level of factor distribution of polishing

Factor		Level		
		−1	0	1
1	ω/r/min	5000	6000	7000
2	a_p/mm	0.6	0.9	1.2
3	v_f/mm/min	120	160	200
4	P	240	320	400

Table 3 Experiments and results of central composite design

Number	Level				Result
	ω	a_p	v_f	P	
1	5000	0.6	120	240	0.715
2	7000	0.6	120	240	0.671
3	5000	1.2	120	240	0.710
4	7000	1.2	120	240	0.601
5	5000	0.6	200	240	0.733
6	7000	0.6	200	240	0.720
7	5000	1.2	200	240	0.713
8	7000	1.2	200	240	0.634
9	5000	0.6	120	400	0.691
10	7000	0.6	120	400	0.679
11	5000	1.2	120	400	0.681
12	7000	1.2	120	400	0.576
13	5000	0.6	200	400	0.692
14	7000	0.6	200	400	0.691
15	5000	1.2	200	400	0.677
16	7000	1.2	200	400	0.618
17	5000	0.9	160	320	0.606
18	7000	0.9	160	320	0.559
19	6000	0.6	160	320	0.611
20	6000	1.2	160	320	0.566
21	6000	0.9	120	320	0.536
22	6000	0.9	200	320	0.551
23	6000	0.9	160	240	0.581
24	6000	0.9	160	400	0.556
25	6000	0.9	160	320	0.541
26	6000	0.9	160	320	0.548
27	6000	0.9	160	320	0.551
28	6000	0.9	160	320	0.550
29	6000	0.9	160	320	0.539

parameters (P, ω, a_p and v_f) under different levels. Therefore, Eq. (1) can be rewritten as:

$$y = a + b_1\omega + b_2 a_p + b_3 v_f + b_4 P + b_{12}\omega a_p + b_{13}\omega v_f + b_{14}\omega P + b_{23} a_p v_f + b_{24} a_p P + b_{34} v_f P + b_{11}\omega^2 + b_{22} {a_p}^2 + b_{33} {v_f}^2 + b_{44} P^2 \quad (2)$$

Regression coefficients in Eq. (2) can be obtained from the multi-element quadratic nonlinear regression data in Table 3. In other words, multi-element regression model between processing parameters and roughness ratio can be obtained, as follows:

$$y = 3.35005 - 5.61136E{-}004 \times \omega - 0.72732 \times a_p - 1.74295E{-}003 \times v_f - 3.37234E{-}003 \times P - 5.89583\text{E-}005 \times \omega \times a_p + 1.85938\text{E-}007 \times \omega \times v_f + 5.39062\text{E-}008 \times \omega \times P - 2.60417\text{E-}005 \times a_p \times v_f - 4.94792\text{E-}005 \times a_p \times P - 1.03516E{-}006 \times v_f \times P + 4.50906\text{E-}008 \times \omega^2 + 0.56767 \times {a_p}^2 + 3.80663\text{E-}006 \times {v_f}^2 + 4.85791\text{E-}006 \times P^2 \quad (3)$$

3.2 Significance of the prediction model

The significance of the prediction model was verified by variance analysis (Table 4).

The confidence coefficient was set at 95 %. In F-test, the statistics of the model was $F = 176.43 > F_{0.01}(4, 24) = 4.22$, indicating that the prediction model is very significant. Under noise interference, the model shows only 0.01 % possibility to achieve $F = 176.43$. The tested loss-faulty of the model was $F = 2.08$, demonstrating that the loss-faulty of the model is not significant. According to significance test and loss-faulty test results of the model, the regression model can fit well with test results on test points and test values within the whole range. The coefficient of determination (R^2) and the adjusted multiple correlation coefficient (Adj R^2) of the model were 0.9944 and 0.9887, indicating high degree of fitting of the model, consistent with the F-test results. If p value <0.01 (p value is the partial regression coefficient of the model), it extremely significantly influences the prediction model. If $0.01 < p$ value <0.05, it significantly influences the prediction model. If p value >0.05, it influences the prediction model slightly. The variance analysis demonstrated that ω, a_p, P, v_f, ωa_p, ωv_f, ωP, ω^2, ${a_p}^2$ and P^2 are the eight significant influencing factors of the prediction model. Numerous significant influencing factors affect the prediction model, demonstrating that the second-order prediction model is reasonable. Signal-to-noise ratio of the prediction model was represented by Adeq Precision = 36.325 > 4, indicating that the model displays an adequate resolution. To sum up, this prediction model can be used to predict roughness ratio of surfaces polished by abrasive cloth wheels.

Table 4 ANOVA table for the regression model

Source	Sum of squares	*df*	Mean square	*F* value	*p* value Prob > *F*
Model	0.13	14	9.30E-03	176.43	<0.0001
A-w	0.012	1	0.012	232.83	<0.0001
B-ap	0.01	1	0.01	193.08	<0.0001
C-vf	1.61E-03	1	1.61E-03	30.46	<0.0001
D-P	2.59E-03	1	2.59E-03	49.18	<0.0001
AB	5.01E-03	1	5.01E-03	94.97	<0.0001
AC	8.85E-04	1	8.85E-04	16.79	0.0011
AD	2.98E-04	1	2.98E-04	5.65	0.0323
BC	1.56E-06	1	1.56E-06	0.03	0.8658
BD	2.26E-05	1	2.26E-05	0.43	0.5235
CD	1.76E-04	1	1.76E-04	3.33	0.0894
A^2	5.26E-03	1	5.26E-03	99.74	<0.0001
B^2	6.75E-03	1	6.75E-03	128.05	<0.0001
C^2	9.59E-05	1	9.59E-05	1.82	0.1988
D^2	2.50E-03	1	2.50E-03	47.42	<0.0001
Residual	7.38E-04	14	5.27E-05		
Lack of fit	6.19E-04	10	6.19E-05	2.08	0.2496
Pure error	1.19E-04	4	2.97E-05		
Cor total	0.13	28			

Std. Dev. = 7.260E-003, Mean = 0.62, *C.V.* % = 1.16, PRESS = 4.028E-003, R^2 =0.9944, Adj R^2 =0.9887, Pred R^2 =0.9692, Adeq Precision = 36.326; *df* degrees of freedom, *CV* coefficient of variation, *F* Fisher's ratio, *p* probability

4 Optimization and verification of processing parameters

4.1 Optimization of parameters

The influence laws on surface roughness ratio can be determined by substituting zero-level values of every factor into Eq. (3) (Fig. 6).

Figure 6(a), (b) shows that the surface roughness ratio decreases first and then increases as ω and a_p increase. Moreover, the number of abrasive particles participating in polishing per unit area and unit time, as well as the polishing force, increases, thereby increasing material removal. However, when a_p increases to radius increment Δr, the stability and flexibility of the abrasive cloth wheel decrease, making a nearly rigid contact with the workpiece surface. This phenomenon easily causes vibration-induced uneven polishing and increases the surface roughness ratio. Figure 6(c) shows that the roughness ratio is positively correlated with feed speed v_f because when the feed speed increases, polishing time per unit area and the number of involved abrasive particles are reduced, whereas the grinding thickness of single abrasive particle increases and the surface plastic deformation intensifies. In Fig. 6(d), roughness ratio decreases first and then increases with increasing abrasive size *P*. This phenomenon occurs because a high abrasive size *P* will involve more abrasive particles during grinding and reduce the grinding thickness of single abrasive particle, whereas a considerably high abrasive size results in few amount of removed material and in reduced polishing efficiency on a rough surface. Based on the valley points of curves in

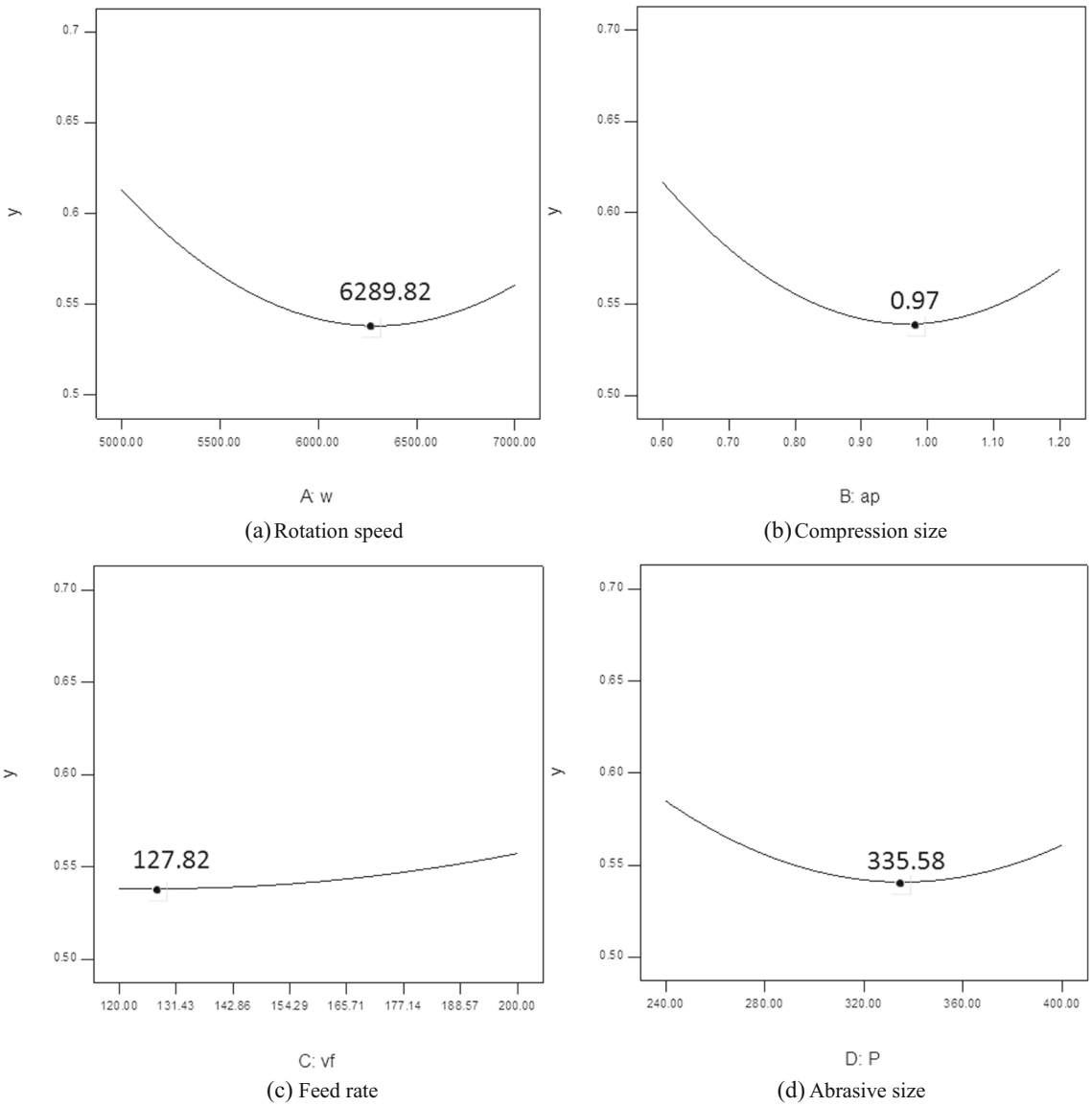

Fig. 6 Trend of changes in surface roughness ratio as a function of a single parameter

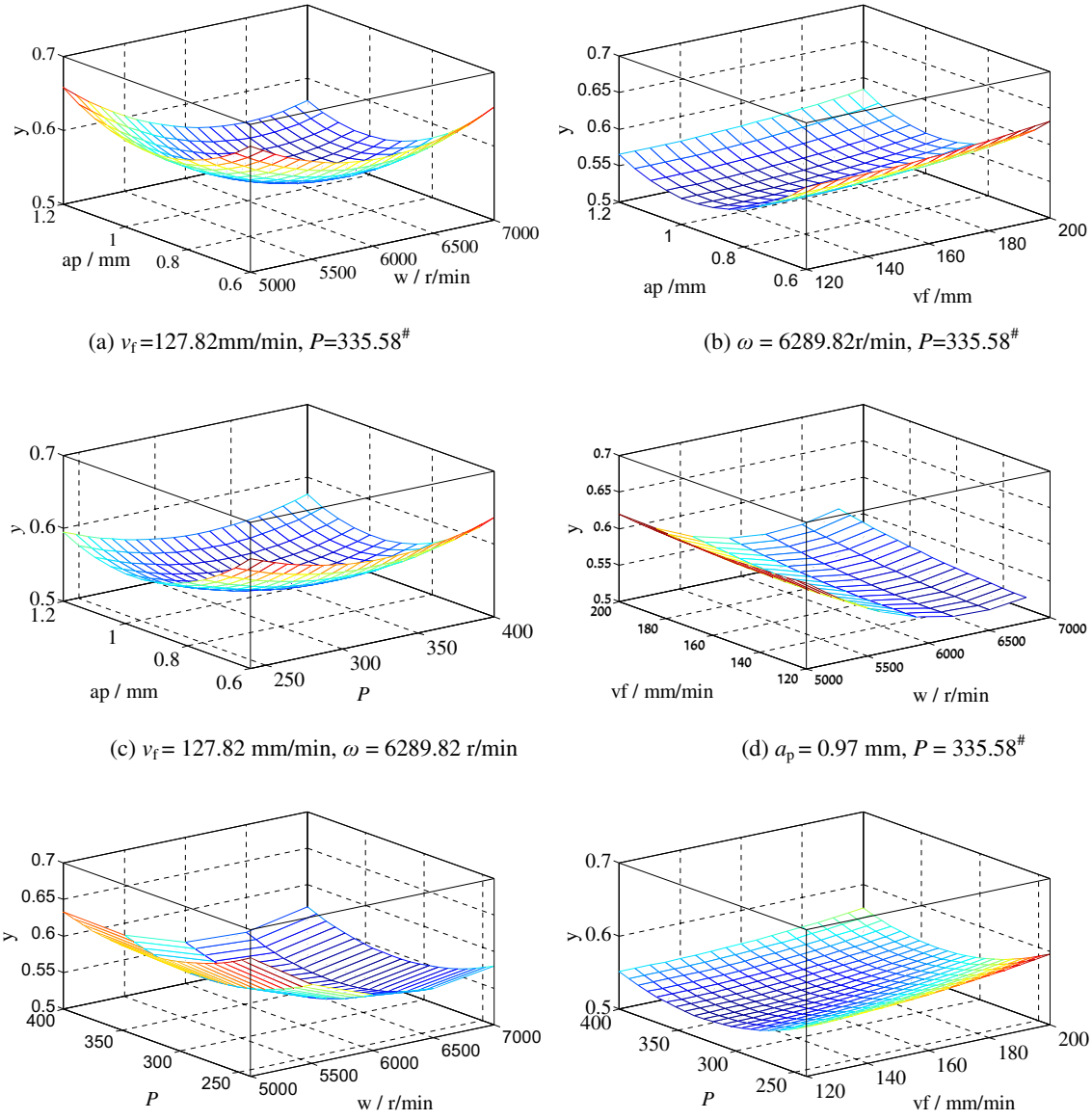

(a) v_f=127.82mm/min, P=335.58$^{\#}$

(b) ω = 6289.82r/min, P=335.58$^{\#}$

(c) v_f = 127.82 mm/min, ω = 6289.82 r/min

(d) a_p = 0.97 mm, P = 335.58$^{\#}$

(e) a_p = 0.97 mm, v_f = 127.82 mm/min

(f) ω = 6289.82 r/min, a_p = 0.97 mm

Fig. 7 The response surface for the optimal level of each single factor

Fig. 6, the optimum theoretical values of ω, a_p, v_f and P are 6289.82 r/min, 0.97 mm, 127.82 mm/min and 335.58$^{\#}$, respectively. In fact, setting the value of ω at 6289.82 r/min is difficult, and an abrasive size of 335.58$^{\#}$ does not exist in the actual abrasive size specification. y = 0.5375 when ω = 6250 r/min; y = 0.5374 when ω = 6300 r/min; y = 0.5376 when ω = 6350 r/min. Therefore, the optimum practical value of ω is 6300 r/min, and the optimum practical value of P is 320$^{\#}$.

The response surface could be acquired by Matlab software (Fig. 7) based on the theoretical optimal values of all factors and combined with Eq. (3). Figure 7 shows the coupling effect of processing parameters on surface roughness ratio.

In Fig. 7(a), y shows a V-shaped variation when a_p and ω increase. When a_p = 0.99 mm and ω = 6406.90 r/min, y_{min} = 0.5270. Given the low a_p and ω, fewer abrasive particles are involved in polishing, and the polishing force is weak, resulting in small material removal. When ω and a_p continue to increase, the number of abrasive particles that participate in polishing per unit area and unit time, as well as the polishing force, increases, thereby increasing the material removal and reducing roughness ratio. However, when a_p is greater than the radius increment (Δr), rigidity of abrasive cloth wheel becomes great, whereas stability and flexibility of the abrasive cloth wheel decrease, resulting in its nearly rigid contact with the workpiece surface. This phenomenon also easily causes

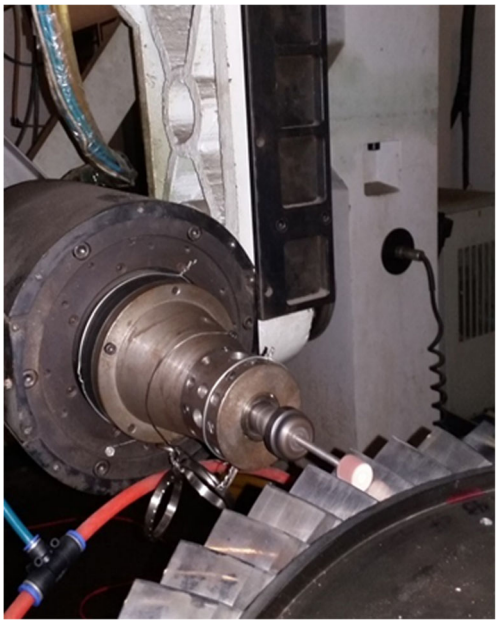

Fig. 8 Polishing test

Fig. 9 Comparison of polishing effect

vibration-induced uneven polishing and increases the surface roughness ratio.

In Fig. 7(b), y increases with increasing v_f, although it decreases first and then increases as a_p increases. When $a_p = 0.99$ mm and $v_f = 124.33$ mm/min, $y_{min} = 0.5275$. As v_f increases, number of abrasive particles participating in polishing per unit area and time decreases, whereas number of involved abrasive particles and polishing force increase as a_p increases. However, the continuous increase in a_p will intensify the rigidity of the abrasive cloth wheel, resulting in vibrations and uneven polishing.

In Fig. 7(c), y shows a V-shaped variation when P and a_p increase. When $a_p = 0.98$ mm and $P = 330.83^{\#}$, $y_{min} = 0.5275$. A higher P is accompanied by an increased number of abrasive particles involved during polishing; however, as P continuously increase, material removal decreases and the polishing efficiency declines. Similar influencing law was observed in a_p.

Similar influencing laws of processing parameters on y were observed in Fig. 7(d)–(f). In Fig. 7(d), $y_{min} = 0.5271$ when $\omega = 6404.82$ r/min and $v_f = 121.43$ mm/min. In Fig. 7(e), $y_{min} = 0.5271$ when $\omega = 6394.68$ r/min and $P = 330.17^{\#}$. In Fig. 7(f), $y_{min} = 0.5275$ when $P = 330.37^{\#}$ and $v_f = 123.52$ mm/min.

Table 5 Polishing test results

Blade	Roughness/um		y value
	Before polishing	After polishing	
1	1.052	0.555	0.5279
2	0.943	0.497	0.5266
3	0.691	0.364	0.5271
4	0.732	0.387	0.5283

As shown in Fig. 7, the optimum theoretical values of the processing parameters are $\omega = 6434.18$ r/min, $a_p = 0.99$ mm, $v_f = 120$ mm/min and $P = 328.59^{\#}$, when $y = 0.5266$. However, $P = 328.59^{\#}$ is beyond the specifications ($240^{\#}$, $320^{\#}$, and $400^{\#}$) of abrasive cloth wheel and setting the rotation speed at 6434.18 r/min is difficult. After calculation, when $P = 320^{\#}$ and $\omega = 6400$ r/min, the surface roughness ratio is at the minimum ($y_{min} = 0.5271$) Therefore, the practical optimum values of the processing parameters are $\omega = 6400$ r/min, $a_p = 0.99$ mm $P = 320^{\#}$ and $v_f = 120$ mm/min, when $y = 0.5271$.

4.2 Polishing test

A polishing test based on four TC4 blades (Nos. 1, 2, 3, and 4) on the blisk was performed using the practical optimized parameters (Fig. 8) obtained by response surface method. Spacing between polishing routes is $p = 1.2$ mm. Isoparametric line method [19] was employed for track planning. As shown in Fig. 4, the radius of the abrasive cloth wheel (8.5 mm × 14 mm × $320^{\#}$) when $\omega = 6400$ r/min is 10.5 mm. Therefore, the cutter radius in the CNC program is $r\text{-}a_p = 10.5–0.99 = 9.51$ mm. Given that horizontal line spacing method can effectively eliminate external waviness of the blade [20], horizontal line spacing-based polishing, that is, polishing along the milling track, was employed in this paper.

Five measuring points were randomly chosen from the polishing zones. Surface roughness was measured by a Mar Surf XR 20 surface roughometer (sampling length = 0.8 mm and evaluation length = 4 mm) by using the vertical polishing

track approach. The mean value was taken as the final result (Table 5). Based on the polishing results, this prediction model is reliable and could accurately predict roughness ratio of the polishing surface. Furthermore, the optimized parameters could contribute ideal polishing effect (Fig. 9).

5 Conclusions

1) The order of importance of the processing parameters of the abrasive cloth wheel was determined using orthogonal test and range analysis. P is the most important factor, followed by ω, a_p, v_f and p successively. The correlation analysis demonstrates a significant linear correlation between R_a and R'_a ($\rho = 0.932$).

2) The range of processing parameters for orthogonal central combination test was determined from the tendency chart. On this basis, the prediction model of roughness ratio was established and verified significant by variance analyses. The model can thus be used to predict roughness ratio.
3) This prediction model is used to analyze independent and coupling influencing laws of processing parameters on roughness ratio. In addition, optimized processing parameters were determined using the response surface method.
4) The polishing test result of a blisk demonstrates that the prediction model and optimized parameters are reliable.

References

1. Ho W-H, Tsai J-T, Lin B-T, Chou J-H (2009) Adaptive network-based fuzzy inference system for prediction of surface roughness in end milling process using hybrid Taguchi-genetic learning algorithm. Expert Syst Appl 36:3216–3222. doi:10.1016/j.eswa.2008.01.051
2. Huang H, Gong ZM, Chen XQ, Zhou L (2002) Robotic grinding and polishing for turbine-vane overhaul. J Mater Process Technol 127:140–145. doi:10.1016/S0924-0136(02)00114-0
3. Duan JH, Shi YY, Li XBZJ (2011) Adaptive polishing for blisk by flexible grinding head. Acta Aeronaut Astronaut Sin 32:934–940 doi: 1000-6893(2011)05-0934-07
4. Bigerelle M, Gautier A, Hagege B, et al. (2009) Roughness characteristic length scales of belt finished surface. J Mater Process Technol 209:6103–6116. doi:10.1016/j.jmatprotec.2009.04.013
5. Wang G, Wang Y, Zhang L, et al. (2014) Development and polishing process of a mobile robot finishing large mold surface. Mach Sci Technol 18:603–625. doi:10.1080/10910344.2014.955372
6. Márquez JJ, Pérez JM, Ríos J, Vizán A (2005) Process modeling for robotic polishing. J Mater Process Technol 159:69–82. doi:10.1016/j.jmatprotec.2004.01.045
7. Chaves-Jacob J, Linares JM, Sprauel JM (2015) Control of the contact force in a pre-polishing operation of free-form surfaces realised with a 5-axis CNC machine. CIRP Ann - Manuf Technol 64:309–312. doi:10.1016/j.cirp.2015.04.008
8. Ri P, Zhen-Zhong W, Chun-Jin W, et al. (2014) Research on control optimization for bonnet polishing system. Int J Precis Eng Manuf 15:483–488. doi:10.1007/s12541-014-0361-6
9. Zeng S, Blunt L (2014) Experimental investigation and analytical modelling of the effects of process parameters on material removal rate for bonnet polishing of cobalt chrome alloy. Precis Eng 38:348–355. doi:10.1016/j.precisioneng.2013.11.005
10. Ji SM, Jin MS, Zhang X, Zhang L, Zhang YDYJ (2007) Novel gasbag polishing technique for free form mold. J Chem Inf Model 43:2–6. doi:10.1017/CBO9781107415324.004
11. Wang YQ, Yin SH, Huang H, et al. (2015) Magnetorheological polishing using a permanent magnetic yoke with straight air gap for ultra-smooth surface planarization. Precis Eng 40:309–317. doi:10.1016/j.precisioneng.2014.11.001
12. Lee ES, Lee SG, Choi WK, Choi SG (2013) Study on the effect of various machining speeds on the wafer polishing process. J Mech Sci Technol 27:3155–3160. doi:10.1007/s12206-013-0836-x
13. Zhong ZW (2008) Recent advances in polishing of advanced materials. Mater Manuf Process 23:449–456. doi:10.1080/10426910802103486
14. Givi M, Fadaei Tehrani A, Mohammadi A (2012) Polishing of the aluminum sheets with magnetic abrasive finishing method. Int J Adv Manuf Technol 61:989–998. doi:10.1007/s00170-011-3753-0
15. Li M, Lyu B, Yuan J, et al. (2015) Shear-thickening polishing method. Int J Mach Tools Manuf 94:88–99. doi:10.1016/j.ijmachtools.2015.04.010
16. Zhao T, Shi Y, Lin X, et al. (2014) Surface roughness prediction and parameters optimization in grinding and polishing process for IBR of aero-engine. Int J Adv Manuf Technol 74:653–663. doi:10.1007/s00170-014-6020-3
17. Zhsao P, Shi Y (2013) Composite adaptive control of belt polishing force for aero-engine blade. Chinese J Mech Eng 26:988–996. doi:10.3901/CJME.2013.05.988
18. Sun Y, Giblin DJ, Kazerounian K (2009) Accurate robotic belt grinding of workpieces with complex geometries using relative calibration techniques. Robot Comput Integr Manuf 25:204–210. doi:10.1016/j.rcim.2007.11.005
19. Lin XJ, Yang Y, Wu G, Gao Y, Chen Y, Liu MLM (2015) The research of flexible polishing technology of five-axis NC abrasive belt for blade surface. Acta Aeronaut Astronaut Sin 36:2074–2082. doi:10.7527/S1000-6893.2014.0203
20. Duan JH, Shi YY, Zhang JF, Dong TLX (2012) Flexible polishing technology for blade of aviation engine. Acta Aeronaut Astronaut Sin 33:573–578 doi: cnki:11-1929/v.20111014.1505.004
21. Yong Y, Kulkarni SS, Rys M, Lei S (2012) Development of a surface roughness model in end milling of nHAP using PCD insert. Ceram Int 38:6865–6871. doi:10.1016/j.ceramint.2012.05.087
22. Hanafi I, Khamlichi A, Cabrera FM, Nuñez López PJ (2012) Prediction of surface roughness in turning of PEEK cf30 by using an artificial neural network. J Chinese Inst Ind Eng 29:337–347. doi:10.1080/10170669.2012.702690
23. Singh D, Rao PV (2007) A surface roughness prediction model for hard turning process. Int J Adv Manuf Technol 32:1115–1124. doi:10.1007/s00170-006-0429-2
24. Bigerelle M, Hagege B, El Mansori M (2008) Mechanical modelling of micro-scale abrasion in superfinish belt grinding. Tribol Int 41:992–1001. doi:10.1016/j.triboint.2008.03.015